Acta Pharmaceutica Sinica B 2025;15(7):3632−3645

Chinese Pharmaceutical Association
Institute of Materia Medica, Chinese Academy of Medical Sciences

Acta Pharmaceutica Sinica B

www.elsevier.com/locate/apsb
www.sciencedirect.com

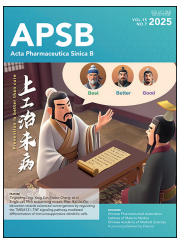

ORIGINAL ARTICLE

Linagliptin synergizes with cPLA2 inhibition to enhance temozolomide efficacy by interrupting DPP4-mediated EGFR stabilization in glioma

Dongyuan Su[a,†], Biao Hong[a,†], Shixue Yang[a,†], Jixing Zhao[a], Xiaoteng Cui[a], Qi Zhan[a], Kaikai Yi[b], Yanping Huang[a], Jiasheng Ju[a], Eryan Yang[c], Qixue Wang[a], Junhu Zhou[a], Yunfei Wang[a], Xing Liu[d,*], Chunsheng Kang[a,*]

[a]*Department of Neurosurgery, Tianjin Medical University General Hospital, Laboratory of Neuro-oncology, Tianjin Neurological Institute, Key Laboratory of Post-Neuro Injury Neuro-Repair and Regeneration in Central Nervous System, Ministry of Education and Tianjin City, Tianjin 300052, China*
[b]*Department of Neuro-Oncology and Neurosurgery, Tianjin Medical University Cancer Institute and Hospital, National Clinical Research Center for Cancer, Key Laboratory of Cancer Prevention and Therapy of Tianjin, Tianjin's Clinical Research Center for Cancer, Tianjin 300060, China*
[c]*Department of Gynecology and Obstetrics, Tianjin Medical University General Hospital, Tianjin 300052, China*
[d]*Department of Neuropathology, Beijing Neurosurgical Institute, Capital Medical University, Beijing 100070, China*

Received 26 June 2024; received in revised form 28 October 2024; accepted 20 December 2024

KEY WORDS

Glioblastoma;
PTRF;
cPLA2;
DPP4;
EGFR;
Linagliptin;
Lipid remodeling;
Novel therapy

Abstract The polymerase 1 and transcript release factor (PTRF)−cytoplasmic phospholipase A2 (cPLA2) phospholipid remodeling pathway facilitates tumor proliferation in glioma. Nevertheless, blockade of this pathway leads to the excessive activation of oncogenic receptors on the plasma membrane and subsequent drug resistance. Here, CD26/dipeptidyl peptidase 4 (DPP4) was identified through screening of CRISPR/Cas9 libraries. Suppressing PTRF−cPLA2 signaling resulted in the activation of the epidermal growth factor receptor (EGFR) pathway through phosphatidylcholine and lysophosphatidylcholine remodeling, which ultimately increased DPP4 transcription. In turn, DPP4 interacted with EGFR and prevented its ubiquitination. Linagliptin, a DPP4 inhibitor, facilitated the degradation of EGFR by blocking its interaction with DPP4. When combined with the cPLA2 inhibitor AACOCF3, it exhibited

*Corresponding authors.
E-mail addresses: liuxing_bjni@mail.ccmu.edu.cn (Xing Liu), kang97061@tmu.edu.cn (Chunsheng Kang).
[†]These authors made equal contributions to this work.
Peer review under the responsibility of Chinese Pharmaceutical Association and Institute of Materia Medica, Chinese Academy of Medical Sciences.

https://doi.org/10.1016/j.apsb.2025.05.012

synergistic effects and led to a decrease in energy metabolism in glioblastoma cells. Subsequent *in vivo* investigations provided further evidence of a synergistic impact of linagliptin by augmenting the sensitivity of AACOCF3 and strengthening the efficacy of temozolomide. DPP4 serves as a novel target and establishes a constructive feedback loop with EGFR. Linagliptin is a potent inhibitor that promotes EGFR degradation by blocking the DPP4−EGFR interaction. This study presents innovative approaches for treating glioma by combining linagliptin with AACOCF3 and temozolomide.

1. Introduction

Glioblastoma (GBM) is the most malignant primary brain tumor, with a median survival of approximately 15 months[1-3]. Despite numerous treatments including immunotherapies, bevacizumab, and viral therapies being researched for GBM, there have been no substantial advancements[4-6]. It is imperative to investigate novel targets that promote the initiation and progression of GBM.

The modification of the phospholipid composition of membranes and cells has functional effects on malignancies[7,8]. The cytoplasmic phospholipase A2 (cPLA2) enzyme breaks down phospholipids to produce fatty acids[9], which are then utilized in the tricarboxylic acid cycle through β-oxidation to generate energy[10]. Our pioneering study revealed that polymerase 1 and transcript release factor (PTRF), an indicator associated with mesenchymal subtype, stabilizes cPLA2 to increase unsaturated lysophosphatidylcholine (LPC) levels and LPC-mediated increases in membrane fluidity, which in turn promotes tumor proliferation and suppresses immune responses in GBM[11,12]. AACOCF3, a cPLA2 inhibitor, can inhibit this process and prolong the survival of tumor-bearing mice[12]. However, saturated phosphatidylcholine (PC) is thought to contribute to the formation of organized regions inside the plasma membrane which contain active signaling complexes, resulting in transduction of oncogenic signals and tumor growth[13,14]. Hence, specific inhibition of the lipid remodeling pathway is an attractive metabolism-targeted strategy for GBM therapy, while maintaining the equilibrium between PC and LPC is crucial for mitigating its adverse consequences.

The objective of this work was to investigate a further strategy to address the accumulation of PC following prolonged exposure to cPLA2 inhibition. Using CRISPR-Cas9 screening, we identified CD26/dipeptidyl peptidase 4 (DPP4) as a synergistic target induced by PTRF−cPLA2 signaling inhibition. DPP4 stabilizes epidermal growth factor receptor (EGFR) by occupying essential amino acid residues that are important for c-Cbl binding to EGFR, and this is a crucial event in the PTRF−cPLA2 lipid remodeling pathway. We also confirmed that the Exon 25−28 (Ex25−28) region of EGFR and the amino acid (AA) 506−766 region of DPP4 are the critical domains for the interaction between EGFR and DPP4. Interestingly, we demonstrated that linagliptin disrupts the DPP4−EGFR interaction and promotes the degradation of EGFR. Linagliptin could also induce a synergistic effect with AACOCF3 in GBM. This study revealed the noncanonical functionality of linagliptin and highlighted the potential of combining linagliptin with AACOCF3 or TMZ as an innovative therapeutic strategy for treating GBM patients stratified according to PTRF−DPP4−PLA2G4A (PDP) scores.

2. Materials and methods

2.1. Genome-wide CRISPR screening

The U87 and U87-PTRF cells were infected with the pooled GeCKOv2 human lentiviral library (GeneChem, Shanghai, China), containing 123,411 sgRNAs targeting 20,914 human genes, at a multiplicity of infection (MOI) of 0.3 to ensure that most cells received only one stably integrated sgRNA cassette. On the second day, puromycin was added to select the positively transduced cells. After 1 week of puromycin selection, the remaining cells were treated with 25 μmol/L AACOCF3 or DMSO, respectively. After another 14 days of treatment, the survival cells were harvested, and genomic DNA was isolated for the amplification of sgRNAs[15]. The mapping ratio (>80%), distribution, evenness, and missing ratio all meet the standards of quality control. Illumina X platform was used for sgRNAs sequencing. MAGeCKFlute was utilized for analyzing raw data[16].

2.2. Lysophosphatidylcholine (LPC) and phosphatidylcholine (PC) content determination

LPC and PC determination were performed using the lysophosphatidylcholine assay kit (Abcam, Cambridge, UK) and the phosphatidylcholine assay kit (Abcam).

2.3. Coimmunoprecipitation (Co-IP)

The cell lysate was prepared from a lysate buffer of NP-40 (Beyotime, Shanghai, China) with 1% PMSF. The supernatant, target antibody and corresponding IgG were incubated at 4 °C overnight. Then, 40 μL of protein A/G magnetic beads (Selleck, TX, USA) was added to the mixture at 4 °C for 2−4 h, and the beads were washed 3 times for a total of 15 min. Finally, Western blot was used to label the target protein. The primary antibodies used are listed in Supporting Information Table S1.

2.4. Seahorse Xfe extracellular flux analysis (mito stress test)

The cells were seeded on a Seahorse XF24 cell culture microplate (Agilent, Santa Clara, CA, USA). The next day, the oxygen consumption rate (OCR) was determined according to the manufacturer's protocol. One hour before the analysis, the cell culture medium was replaced with XF basic medium supplemented with 10 mmol/L glucose, 2 mmol/L glutamine, and 1 mmol/L pyruvate, and the final pH was 7.4. Then, the cell culture microplate was cultured in a 37 °C carbon dioxide-free incubator for 1 h. The following concentrations of drugs were used during OCR

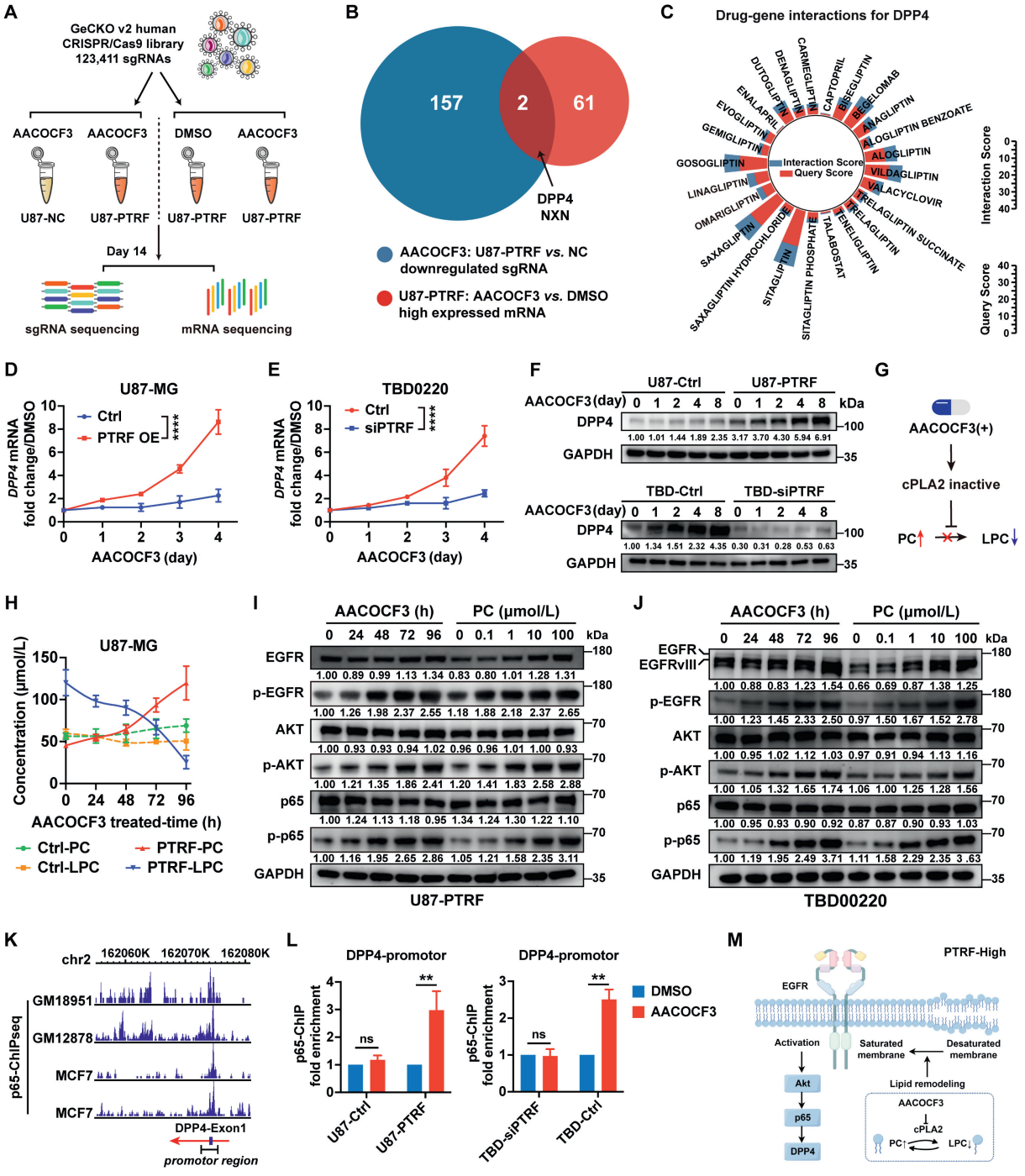

Figure 1 CRISPR-Cas9 library screening revealed that DPP4 is a target that attenuates the cytotoxic effects of AACOCF3 in U87-PTRF cells. (A) Schematic diagram of CRISPR-Cas9 library screening. (B) Candidate genes were obtained through Venn diagram analysis. (C) Drug−gene interaction diagram of *DPP4*. (D, E) The mRNA levels of *DPP4* in U87-MG and TBD0220 cells were treated with 25 μmol/L AACOCF3. (F) DPP4 protein levels in U87-MG and TBD0220 cells after long-term treatment with 25 μmol/L AACOCF3. (G) Schematic model of the role of cPLA2 inhibition in PC/LPC transformation. (H) Quantitative analysis of PC/LPC in U87-MG cells after treatment with 25 μmol/L AACOCF3 for different durations. (I, J) Changes in the levels of EGFR and its downstream proteins in GBM cells after 0−96 h of treatment with 25 μmol/L AACOCF3 or 72 h of treatment with different concentrations of PC. (K) The p65 binding peak in the *DPP4* promoter region in the ChIP-seq database. (L) ChIP-PCR using anti-p65 antibodies in GBM cell lines treated with 25 μmol/L AACOCF3 for 48 h. (M) Mechanistic diagram of AACOCF3-induced PC/LPC lipid remodeling leading to the upregulation of DPP4. Data are represented as mean ± SD; $n = 3$ independent experiments. $^{**}P < 0.01$, $^{****}P < 0.0001$; ns, no significance.

collection: oligomycin (2 μmol/L), short-chain chlorinated paraffin (2 μmol/L), and rotenone/antimycin A mixture (0.5 μmol/L). Extracellular flux experiments were carried out on a hippocampal XF24 analyzer (Agilent). The data were analyzed by Seahorse software.

2.5. *In vivo xenograft mouse models*

All animal research protocols were approved by the Institutional Animal Care and Use Committee (IACUC) of Beijing Tiantan Hospital, Capital Medical University (Approval No. 202204004) according to all animal ethical and safety guidelines. The orthotopic GBM model was established in 4-week-old female BALB/c nude mice. Under the guidance of a stereotaxic apparatus, TBD0220 cells transduced with luciferase lentivirus (1×10^5, dissolved in 3 μL of PBS) were injected into each mouse at 2.0 mm posterior, 2.0 mm lateral, and 3.0 mm ventral to the fontanel to construct an *in situ* GBM model. The mice were examined by bioluminescence imaging of the parietal lobe on the 7th, 14th, and 21st days after tumor transplantation. Survival curves were generated *via* the Kaplan−Meier method. The difference in the survival rates across the groups was analyzed by the logarithmic rank test. At the termination of the animal experiment, the animals were humanely sacrificed, and the intracranial tumor tissues were extracted for IHC and H&E analysis.

2.6. *Human samples and ethics statement*

The research in this study adhered to all ethical and safety regulations. Glioma tissues were obtained from Beijing Tiantan Hospital, Capital Medical University, with written consent from the patients. Approval for this study was granted by the Beijing Tiantan Hospital, Capital Medical University, Ethical Committee (Approval No. KY 2020-131-02, 2022.04.06). Patient selection was unbiased.

2.7. *Statistical analysis*

All bioinformatics analyses and visualizations were performed in R 4.2.1. All the statistical analyses were carried out using GraphPad Prism 8.4.0 software. Student's *t*-test was used to compare 2 experimental groups, while ANOVA was used to compare multiple experimental groups. SynergyFinder (Bliss model) was used to determine the combination score[17]. The graphic abstract was drawn by Figdraw. The error bars in the figures represent mean ± standard deviation (SD) of at least 3 independent experiments ($n = 3$). Significance is indicated as follows: $^*P < 0.05$, $^{**}P < 0.01$, $^{***}P < 0.001$, $^{****}P < 0.0001$, ns = no significance.

2.8. *Other methods*

For materials and methods related to tissue microarrays (TMAs), RNA sequencing, cell culture and drug treatment, Western blot (WB), immunofluorescence (IF) assay, chromatin immunoprecipitation (ChIP), hematoxylin and eosin (H&E) staining and immunohistochemistry (IHC), cell viability and clonogenicity assays, RNA isolation and quantitative real-time PCR (qRT-PCR), siRNA transfection and lentiviral transduction, see Supporting Information for details.

3. Results

3.1. *CRISPR-Cas9 library screening reveals that DPP4 is a target that attenuates the cytotoxic effects of AACOCF3*

To explore the targets related to the cytotoxic effects of AACOCF3, we measured the basal PTRF level of TBD0220 and U87-MG, showing that the PTRF basal level was lower in U87-MG cells (Supporting Information Fig. S1A) and we performed CRISPR/Cas9 library screening of PTRF-overexpressing U87-MG cells (U87-PTRF) and negative control cells (U87-NC) (Fig. S1F). mRNA and sgRNA sequencing analyses were performed on Days 0 and 14 (Fig. 1A, Fig. S1B and S1C). The decreased sgRNA indicates that cells lacking sgRNA-targeted genes are unable to survive, suggesting these genes may contribute to AACOCF3 resistance. Meanwhile, the genes that exhibit increased expression in survived cells after selection may contribute to drug resistance. Therefore, we intersected the differential genes from CRISPR library screening and the genes from mRNA sequencing, resulting in 2 candidate genes (Fig. 1B). To further assess candidate targets, drug−gene interaction (DGI) analyses of the two genes were performed. There were 25 drugs targeting DPP4, but no drugs targeting NXN were identified (Fig. 1C). GO-BP enrichment analysis revealed that genes positively correlated with DPP4 were enriched mainly in the inflammatory response, apoptosis, vesicle-mediated transport, angiogenesis, and the NF-κB signaling pathway (Fig. S1D). Moreover, in the CGGA database, high *DPP4* expression was associated with poorer survival outcomes (Fig. S1E). Therefore, we selected *DPP4* as the gene of interest for subsequent experimental and clinical evaluation.

We used U87-PTRF cells and TBD0220 cells (with high endogenous PTRF) to explore the molecular mechanism of DPP4 elevation under PTRF overexpression and AACOCF3 treatment. We found that under conditions of high PTRF expression, long-term AACOCF3 treatment of GBM cells led to increased *DPP4* mRNA and protein levels, but this phenomenon was not obvious under conditions of low PTRF expression (Fig. 1D−F). AACOCF3 plays a role in blocking cPLA2, an enzyme that mediates the conversion of PC to LPC, which increases PC accumulation (Fig. 1G). We found that under conditions of high PTRF expression, with increasing AACOCF3 treatment time, the degree of accumulation of PC in GBM cells increased, while the production of LPC decreased; however, this phenomenon was not obvious under conditions of low PTRF expression (Fig. 1H and Fig. S1H). Previous studies have shown that the accumulation of PC in cells can cause phospholipid remodeling in cell membranes, which in turn causes the activation of membrane carcinogenic signals[14]. WB showed that after long-term AACOCF3 treatment in GBM cells with high PTRF expression, p-EGFR was elevated, and p-AKT and p-p65 subsequently increased, which was also observed after PC treatment in GBM cells with high PTRF expression (Fig. 1I and J). We then analyzed the ChIP-seq data in the GEO database (GSM486305 and GSM1643963) and detected a p-p65 enrichment peak in the *DPP4* promoter region, suggesting that *DPP4* may be regulated by p65 (Fig. 1K). Next, we found that

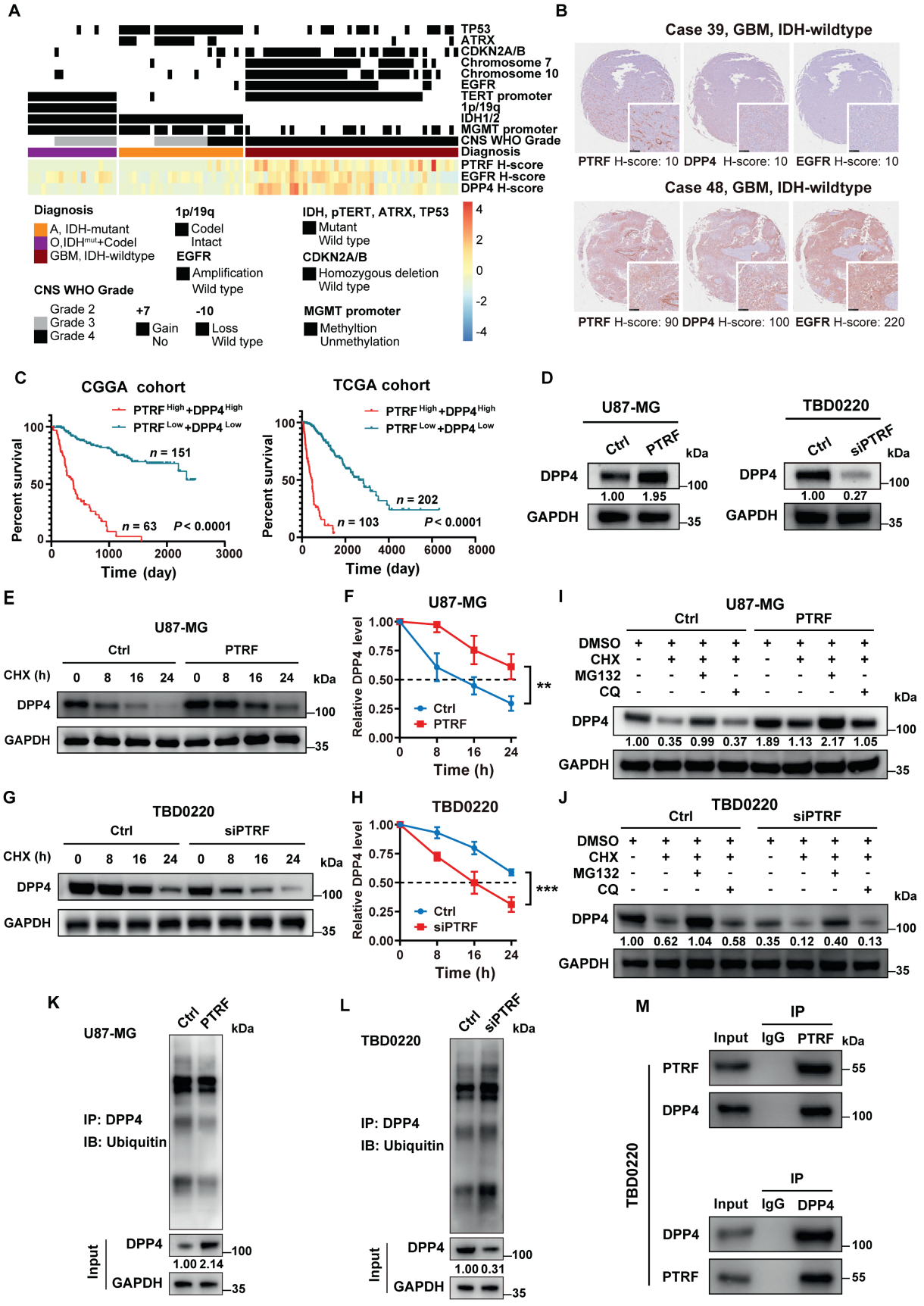

Figure 2 PTRF stabilizes DPP4 and prevents its ubiquitination (A) Heatmap displaying PTRF, EGFR, and DPP4 H-scores among glioma patients with different characteristics. (B) Representative IHC staining of PTRF, EGFR, and DPP4 in GBM patient tissue microarray. (C)

in GBM cells with high PTRF expression, long-term AACOCF3 treatment increased p65 binding to the *DPP4* promoter region, but this effect was not obvious in GBM cells with low PTRF expression (Fig. 1L). In summary, long-term treatment of GBM cells with high PTRF expression with AACOCF3 led to PC/LPC imbalance and activated EGFR-AKT-p65 signaling to induce DPP4 expression (Fig. 1M).

3.2. PTRF prevents DPP4 from being ubiquitinated and stabilizes DPP4

To verify the potential relationship between PTRF and DPP4, we analyzed cohorts from the TCGA and CGGA databases. The results indicated that PTRF expression was positively correlated with DPP4 expression and that the expression of DPP4 and PTRF tended to increase with increasing histological grade (Supporting Information Fig. S2A−S2D). To determine the clinical significance of DPP4, we further analyzed TMAs. The H-score of PTRF was positively correlated with the H-score of DPP4 (Fig. S2E). In addition, DPP4 and PTRF H-scores were vastly elevated in GBM. These results suggested that DPP4 and PTRF expression may contribute to GBM tumorigenesis (Fig. 2A and B, Fig. S2F). Gene expression profile analysis of TCGA and CGGA data indicated that patient prognosis was negatively correlated with PTRF and DPP4 expression (Fig. 2C). Therefore, high PTRF and DPP4 expression is a poor prognostic factor for glioma patients, which further supports the potential value of targeting DPP4 in glioma. As our previous study reported, PTRF can prevent the ubiquitination of specific proteins[12,18]. To verify the regulatory effect of PTRF on DPP4, we overexpressed PTRF in U87-MG (U87-PTRF) cells and knocked down PTRF in TBD0220 cells (Fig. S1F and S1G). We found that the overexpression and knockdown (KD) of PTRF affected the protein level of DPP4 (Fig. 2D). By applying a protein synthesis inhibitor (CHX), we verified that DPP4 degradation occurred faster when PTRF expression was low (Fig. 2E−H). These results indicated the post-transcriptional regulation of PTRF on DPP4. Because DPP4 degradation could be regulated by autophagy or the ubiquitin−proteasome system (UPS), the two main proteolytic systems, U87-PTRF cells and TBD0220 cells with PTRF KD, were treated with the lysosomal inhibitor CQ, the proteasome inhibitor MG132, or CHX for 24 h to determine which proteolytic system regulates DPP4 protein degradation. WB analysis revealed that, in the presence or absence of PTRF, DPP4 was strongly degraded upon treatment with CHX, and this degradation was reversed by treatment with MG132 but not CQ (Fig. 2 I and J). These results indicate that DPP4 is degraded only by the UPS and that PTRF does not affect the manners of DPP4 degradation.

Finally, Co-IP assays were performed and indicated that DPP4 was more easily ubiquitinated when PTRF was depleted, while the ubiquitination of DPP4 decreased with PTRF overexpression (Fig. 2K and L). Furthermore, PTRF and DPP4 could interact with each other directly according to cross-IP experiments with anti-PTRF or anti-DPP4 antibody (Fig. 2M). Taken together, these data indicate that PTRF prevents DPP4 from being ubiquitinated and thus stabilizes DPP4.

3.3. The AA 506−766 truncation of DPP4 binds to the Ex25−28 truncation of EGFR to prevent c-Cbl interaction with EGFR to stabilize EGFR

We demonstrated that EGFR is a crucial component of the PTRF−cPLA2 phospholipid remodeling pathway. Next, IHC staining of patient brain sections was performed, and we found that DPP4 and EGFR were highly expressed in CNS WHO Grade 4 gliomas. Interestingly, we found that EGFR expression was positively correlated with DPP4 expression through TMA analysis (Fig. 2A and B). *EGFR*, an oncogene, is widely overexpressed and aberrantly activated in diverse tumors, including gliomas, where it promotes tumorigenesis and development, and dysregulation of EGFR protein stability has been reported to critically contribute to abnormal EGFR signaling and cancer development[19]. We further investigated the relationship between DPP4 and EGFR in U87-MG and TBD0220 cells. We found that DPP4 KD decreased the protein level of EGFR/EGFRvIII (Supporting Information Fig. S3A); however, the mRNA level remained stable (Fig. S3B), which indicated that DPP4 regulates the posttranscriptional degradation of EGFR/EGFRvIII. With the combination of CHX, we found that DPP4 KD promoted the degradation of large amounts of EGFR/EGFRvIII, which confirmed the above results (Fig. 3A and B). Then, CQ, MG132, and CHX were applied to determine whether autophagy or the UPS contributed to EGFR/EGFRvIII degradation. WB analysis revealed that, regardless of the presence of DPP4, EGFR and EGFRvIII were strongly degraded upon treatment with CHX, and this degradation was attenuated by treatment with MG132 but not CQ (Fig. 3C). Furthermore, IP experiments showed an increasing trend in the level of ubiquitinated EGFR/EGFRvIII when DPP4 was depleted (Fig. 3D and E). Analysis of IF images indicated that there was a low colocalization rate between EGFR/EGFRvIII and lysosomes in the Ctrl-KD and DPP4-KD groups, which indicates that EGFR/EGFRvIII is not degraded *via* lysosomes (Fig. S3C). In addition, immunoprecipitation with anti-EGFR or DPP4 antibodies pulled down both DPP4 and EGFR/EGFRvIII (Fig. 3F). These results demonstrate that EGFR/EGFRvIII are degraded mainly through the UPS without EGF stimulation and EGFR/EGFRvIII is stabilized and protected from ubiquitination-mediated degradation when bound to DPP4.

To further map the interaction domain of EGFR and DPP4, we constructed a series of EGFR and DPP4 truncation mutants and

Kaplan−Meier survival analysis based on the expression levels of *PTRF* and *DPP4* in the CGGA and TCGA cohorts. (D) Protein levels of DPP4 in U87-PTRF and in TBD0220 cells with PTRF KD. (E, F) WB analysis and quantification of DPP4 degradation in Ctrl- and PTRF-overexpressing U87-MG cells treated with CHX for 24 h. (G, H) WB analysis and quantification of DPP4 degradation in Ctrl- and PTRF-KD-TBD0220 cells treated with CHX for 24 h. (I) DPP4 protein levels in Ctrl- and PTRF-overexpressing U87-MG cells treated with CHX, MG132, or CQ for 24 h. (J) Protein level of DPP4 in Ctrl- and PTRF-KD-TBD0220 cells treated with CHX, MG132, or CQ for 24 h. (K) Co-IP assays were conducted with an anti-DPP4 antibody in Ctrl- and PTRF-overexpressing U87-MG cells, followed by immunoblotting with ubiquitin. (L) Co-IP assays were conducted with an anti-DPP4 antibody in Ctrl- and PTRF-KD-TBD0220 cells, followed by immunoblotting with ubiquitin. (M) The association between PTRF and DPP4 was determined by Western blot with anti-PTRF and anti-DPP4 antibodies. Data are represented as mean ± SD; $n = 3$ independent experiments. $^{**}P < 0.01$ and $^{***}P < 0.001$.

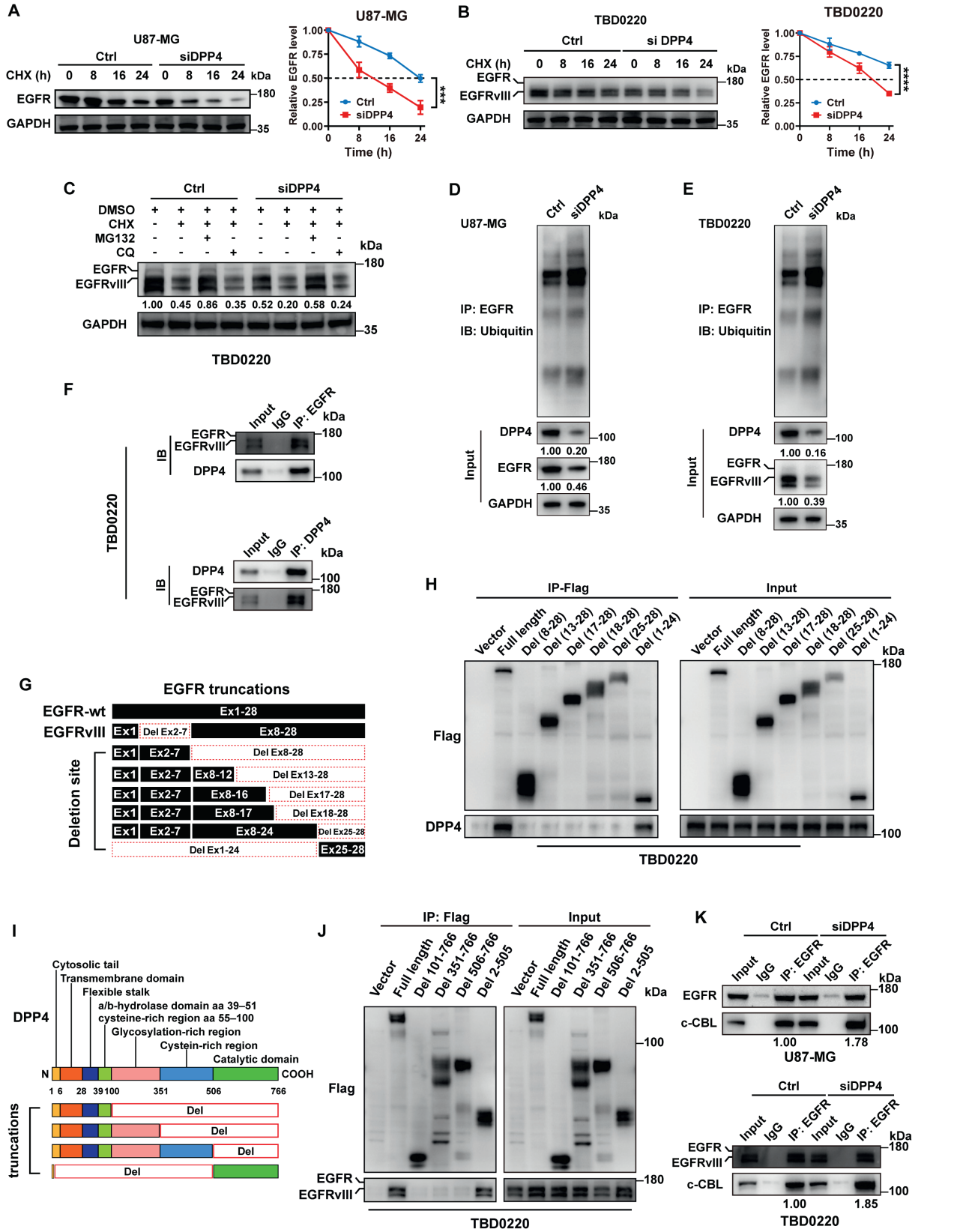

Figure 3 DPP4 interacts with EGFR/EGFRvIII to prevent its ubiquitination. (A, B) WB analysis and quantification of EGFR/EGFRvIII degradation in Ctrl- and DPP4-KD-U87-MG and TBD0220 cells treated with CHX for 24 h. (C) Protein levels of EGFR/EGFRvIII in Ctrl- and DPP4-KD-TBD0220 cells treated with CHX, MG132, or CQ for 24 h. (D, E) Co-IP assays were conducted with an anti-EGFR antibody in Ctrl- and DPP4-KD-U87-MG and TBD0220 cells, followed by immunoblotting with ubiquitin. (F) The association between EGFR/EGFRvIII and DPP4 was determined by Western blot with anti-EGFR and anti-DPP4 antibodies. (G) Mapping of full-length EGFR/EGFRvIII and its truncated

transfected them into the U87-MG and TBD0220 cell lines (Fig. 3G and I). Co-IP assays with an anti-Flag antibody showed that full-length EGFR and DPP4 could bind to DPP4 and EGFR/EGFRvIII, respectively. In addition, only the Ex25−28 truncation of EGFR and the AA 506−766 truncation of DPP4 interacted with DPP4 and EGFR/EGFRvIII, separately, and the other truncations scarcely captured DPP4 or EGFR/EGFRvIII (Fig. 3H and J, Fig. S3D and S3E). Because EGFRvIII can bind to DPP4, which indicates that Ex2−7 of EGFR does not interact with DPP4, these results indicated that the Ex25−28 region of EGFR and the AA 506−766 region of DPP4 are the key domains involved in the interaction between EGFR and DPP4.

Because Tyr1045 of EGFR is a crucial residue for c-Cbl binding, leading to the ubiquitination of EGFR[20], and because this residue is present in the Ex25−28 region of EGFR, we investigated whether the binding of DPP4 to EGFR prevents c-Cbl from interacting with EGFR/EGFRvIII. Co-IP experiments showed that c-Cbl binding with EGFR/EGFRvIII increased when DPP4 was knocked down compared to that in the Ctrl group (Fig. 3K). Collectively, these results demonstrate that DPP4 can stabilize EGFR/EGFRvIII by competing with c-Cbl for binding of EGFR/EGFRvIII, leading to reduced ubiquitination of EGFR/EGFRvIII.

3.4. Linagliptin promotes EGFR and EGFRvIII degradation through the ubiquitin−proteasome pathway by interrupting the EGFR/EGFRvIII-DPP4 interaction

As a DPP4 inhibitor, linagliptin forms hydrogen bonds with Glu205, Glu206, Tyr662, and Tyr631 of DPP4. In addition, there are aromatic stacking interactions between the xanthine ring system and Tyr547 as well as between the quinazoline ring and Trp629[21]. Some of the key residues are included in the AA 506−766 region of DPP4. Hence, we explored whether linagliptin can block the interaction between DPP4 and EGFR. We carried out cross-IP assays using anti-EGFR and DPP4 antibodies in TBD0220 cells and found that the binding between DPP4 and EGFR/EGFRvIII decreased after 48 h of linagliptin treatment (Fig. 4A and B). DPP4 or EGFR/EGFRvIII were immunoprecipitated in dose- and time-dependent manners, the results showed that after just 8 h and at a concentration as low as 5 μmol/L, linagliptin suppressed the interaction between DPP4 and EGFR/EGFRvIII (Fig. 4C−F). In addition, U87-MG and TBD0220 cells were transfected with an Ex25−28 truncation of EGFR with a tag of Flag and an AA 506−766 truncation of DPP4 with a tag of His and treated with linagliptin for 48 h. Immunoprecipitation of the Ex25−28 truncation of EGFR with an anti-Flag antibody pulled down the reduced His-AA 506−766 truncation of DPP4 after linagliptin treatment compared to that after DMSO treatment (Fig. 4G). These results indicated that linagliptin blocks the binding between the AA 506−766 truncation of DPP4 and the Ex25−28 truncation of EGFR to suppress the interaction between DPP4 and EGFR.

Next, we investigated the effect of linagliptin on the degradation of EGFR in GBM cell lines. As expected, the binding of c-Cbl to EGFR and EGFRvIII increased after linagliptin treatment for 48 h, which suggested that linagliptin may affect its ubiquitination-mediated degradation (Fig. 4H). Additionally, linagliptin reduced the protein level of EGFR but did not influence its mRNA level and promoted the degradation of EGFR/EGFRvIII according to the results for cells treated with both linagliptin and CHX and those treated with CHX alone (Fig. 4C, I and J). U87-MG and TBD0220 cells were treated with CHX, CQ, MG132, or linagliptin to further explore the EGFR/EGFRvIII degradation mechanisms. WB analysis revealed marked degradation following CHX treatment, and this degradation was reversed by treatment with MG132 with or without linagliptin existence (Fig. 4K). Finally, U87-MG and TBD0220 cell pellets were collected 8 h postexposure to linagliptin before EGFR/EGFRvIII was degraded vastly to perform Co-IP assays. As shown in Fig. 4L, the ubiquitination level of EGFR/EGFRvIII was greater in cells treated with linagliptin than in those treated with DMSO. The IF images revealed that EGFR/EGFRvIII scarcely colocalized with lysosomes in the DMSO and linagliptin treatment groups (Fig. S3F). Collectively, these results indicated that linagliptin promotes EGFR/EGFRvIII degradation through the ubiquitin−proteasome pathway by disrupting the interaction between EGFR/EGFRvIII and DPP4.

3.5. Linagliptin synergistically sensitizes GBM cells to AACOCF3 and inhibits energy metabolism and proliferation

We further explored whether the combination of linagliptin and AACOCF3 had a synergistic effect on GBM cells. The dose−response matrix data were analyzed, and we found a clear synergy between these two agents in U87-PTRF and TBD0220 cells (Fig. 5A−D). Next, we found *via* seahorse assays that the combination of the 2 drugs significantly blocked energy production in the U87-PTRF and TBD0220 cell lines (Fig. 5E−L). Interestingly, in U87-Ctrl and TBD-si*PTRF* cells, the combination of linagliptin and AACOCF3 inhibited the mitochondrial respiratory chain and energy production (Supporting Information Fig. S4A−S4H). Moreover, we observed that linagliptin combined with AACOCF3 reversed the increase in ATP production in GBM cells caused by prolonged AACOCF3 treatment (Fig. 5M and N). Subsequent clonogenicity assays also confirmed that linagliptin could synergically sensitize AACOCF3 cells and inhibit GBM cell proliferation (Fig. S4I). Next, we constructed an orthotopic nude mouse GBM model using TBD0220 cells (Fig. 5O). We found that the linagliptin + AACOCF3 group had a lower tumor burden and longer survival than the AACOCF3 group (Fig. 5P−R, Fig. S4J). Analysis of H&E-stained sections of the tumor-bearing mice also revealed that the combined treatment group had the lowest tumor burden (Fig. S4K). IHC staining revealed that the tumor sections of the mice in the combined group had the lowest ki67, EGFR, and DPP4 expression levels (Fig. S4L). Moreover, we used TBD0220 cells to construct the nude mice orthotopic GBM model. One week later, mice were

variants. (H) After TBD cells were transfected with a series of 3 × Flag-tagged EGFR constructs for 48 h, as depicted in (G), Flag Co-IP was conducted to determine the interaction domain of EGFR with DPP4. (I) Mapping of full-length DPP4 and its truncated variants. (J) After TBD0220 cells were transfected with a series of 3 × Flag-tagged DPP4 constructs for 48 h, as depicted in (I), Flag Co-IP was conducted to determine the interaction domain of DPP4 with EGFR/EGFRvIII. (K) Co-IP assays with an anti-EGFR antibody were performed to verify the interaction between EGFR/EGFRvIII and c-Cbl in Ctrl- and DPP4-KD-U87-MG and TBD0220 cells. Data are represented as mean ± SD; $n = 3$ independent experiments. ***$P < 0.001$ and ****$P < 0.0001$.

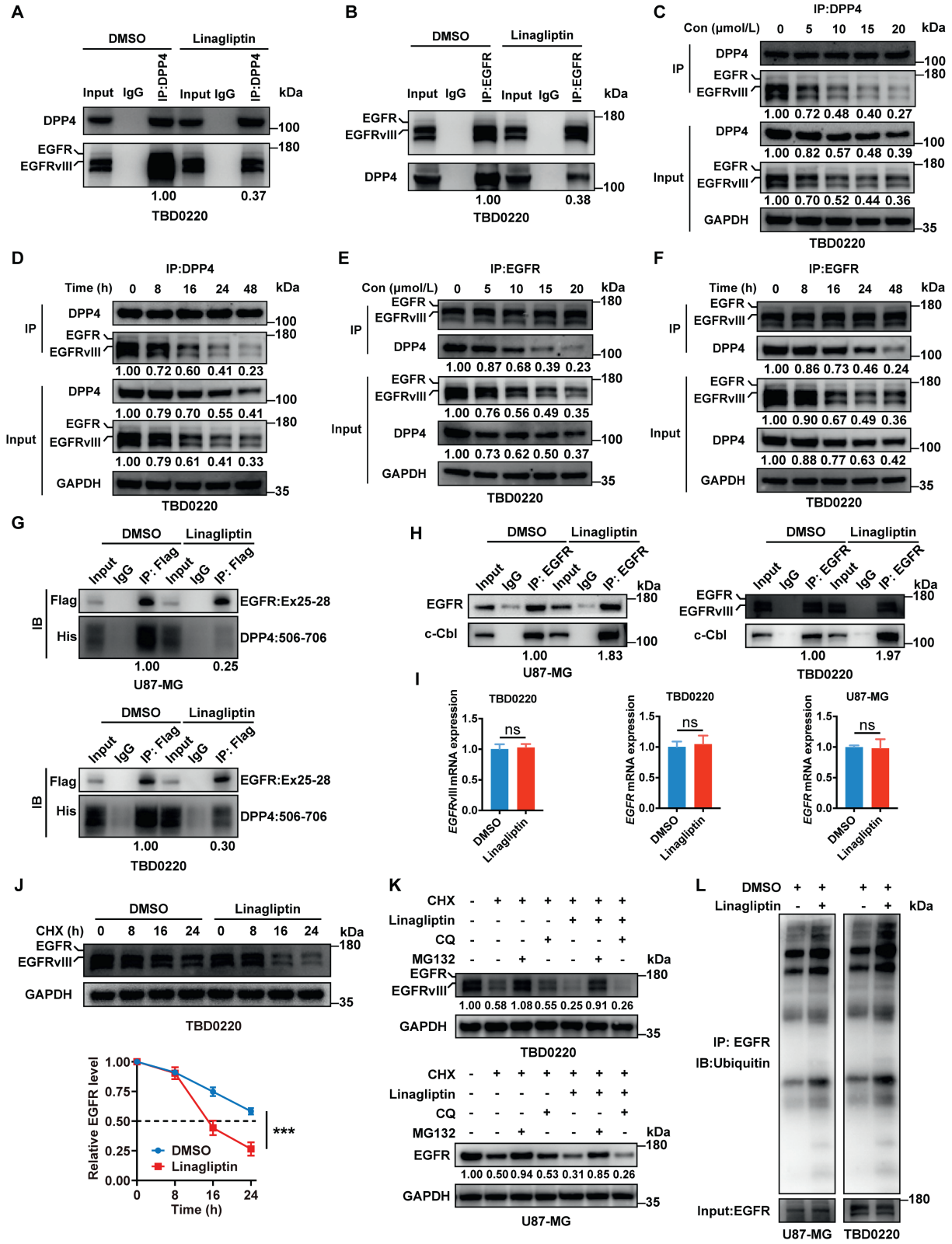

Figure 4 Linagliptin blocks the interaction between EGFR/EGFRvIII and DPP4 to promote EGFR degradation. (A, B) Co-IP assays with anti-DPP4 and anti-EGFR antibodies were performed to verify the interaction between EGFR/EGFRvIII and DPP4 in TBD0220 cells treated with linagliptin (20 μmol/L) for 48 h. (C–F) Co-IP assays with anti-DPP4 and anti-EGFR antibodies in dose- and time-dependent manners to verify the interaction between EGFR/EGFRvIII and DPP4 in TBD0220 cells treated with the indicated concentrations of linagliptin for 48 h or 20 μmol/L linagliptin for the indicated hours. (G) GBM cells were co-transfected with His-AA 506–766 truncation of DPP4 and Flag-Ex25–28 truncation of EGFR and treated with 20 μmol/L linagliptin for 48 h. The association between the His-AA 506–766 truncation of DPP4 and the Flag-Ex25–28

administrated with AACOCF3 (25 mg/kg) and linagliptin (15 mg/kg) and sacrificed humanely in 12 h. Their brain tissues were extracted and divided into brain tumor side and contralateral brain side for liquid chromatography-mass spectrometry (LC−MS) detection. We found that the concentrations of AACOCF3 and linagliptin in brain tumor side tissue were higher than that in contralateral brain side tissue which means that both drugs have good blood−brain barrier permeability and can effectively enrich the tumor area (Fig. S4M and S4N). In summary, we found that linagliptin can enhance the antitumor effect of AACOCF3 both *in vivo* and *in vitro*.

3.6. The combination of linagliptin and AACOCF3 can enhance the antitumor effect of TMZ in vivo

To further investigate the biological and prognostic relevance of *DPP4*, *PTRF*, and *PLA2G4A* (*cPLA2*) expression levels in gliomas, a PDP risk score (PDP score) model was developed, and the PDP score was calculated utilizing the gene expression values and weighted coefficients obtained *via* univariate Cox analysis. We found that the PDP score increased in tandem with the histological grade (Fig. 6A, Supporting Information Fig. S5A and S5B). Moreover, the PDP score was highest in the mesenchymal subtype and lowest in the proneural subtype (Fig. 6B, Fig. S5C and S5D). In addition, we found that the PDP score was elevated in IDH-wildtype lower-grade gliomas (Fig. 6C, Fig. S5E and S5F). We also observed in the TCGA and CGGA cohorts that patients with high PDP score had poorer outcomes (Fig. 6D, Fig. S5G−S5I). Based on the Akaike information criterion, age, WHO grade, IDH status, chromosome 1p/19q status, and PDP score were identified as prognostic factors and were integrated into a nomogram (Fig. 6E). The nomogram yielded a C-index value of 0.874 in the training cohort (TCGA), 0.707 in the CGGA validation cohort and 0.719 in the CGGA#2 validation cohort (Fig. S5J−S5L). The nomogram also showed good calibration in both the training and validation cohorts (Fig. 6F). In conclusion, the assessment of the decision curve demonstrated that among the assessed models, the model based on the combination of clinical features, molecular features, and the PDP score is the most accurate in predicting prognosis.

Next, we evaluated the PDP score of different GBM cell lines by detecting the mRNA levels of *PTRF*, *DPP4*, and *cPLA2*. We found that TBD0220 cells had a high PDP score; these cells were utilized to construct an orthotopic GBM model to investigate the *in vivo* efficacy of the linagliptin + AACOCF3+TMZ triple therapy (Fig. 6G, Supporting Information Fig. S6A). We found that compared with the group treated with TMZ alone, the group treated with linagliptin + AACOCF3+TMZ had a lower tumor burden (Fig. 6H and I) and longer survival (Fig. 6J and K). H&E-stained sections of tumor-bearing mice also showed that the combined group had the lowest tumor burden. IHC staining also showed that the combined group had the lowest ki67 expression (Fig. S6B and S6C). In summary, we found that linagliptin combined with AACOCF3 can enhance the tumor inhibitory effect of TMZ *in vivo*.

4. Discussion

Many novel medications have not demonstrated efficacy in advanced clinical trials for GBM treatment, illustrating gaps in early clinical drug development[22]. Unlike other intracranial tumors that react to small molecular inhibitors targeting cancer signaling pathways, GBM is largely unresponsive to molecular therapies and immune checkpoint inhibitors[23]. With the growing issue of TMZ resistance in GBM patients, new potential targets and treatment approaches for GBM are urgently needed.

Tumor cell proliferation is supported by active metabolic processes[24]. Energy metabolic reprogramming is considered an emerging hallmark of cancer[25,26]. Phospholipids form the structure of cell membranes and are also involved in cellular energy metabolism. In addition to increasing glucose uptake and aerobic glycolysis, lipid metabolic reprogramming enhances the biological behavior of tumor cells[27]. Our previous research revealed that PTRF remodels phospholipids by regulating cPLA2 protein stability and enhancing cPLA2 activity, thereby promoting endocytosis and energy metabolism, intrinsically promoting tumor proliferation, and inhibiting the GBM immune response. Treatment with AACOCF3 and metformin reversed the PTRF−cPLA2 lipid remodeling pathway in GBM[12]. Phospholipase A2 (PLA2) and lysophosphatidylcholine acetyltransferases (LPCATs) are important catalytic enzymes involved in the PC/LPC cycle. cPLA2 catalyzes the conversion of intracellular PC to LPC, and the accumulation of intracellular PC increases when the activity of cPLA2 is inhibited by AACOCF3. Saturated PC has previously been shown to be associated with aggressive histology and a poor prognosis in a large group of breast cancer patients[28]. In GBM, saturated PC mediates cell membrane phospholipid remodeling, further activating oncogenic receptors (EGFR, MET) on the membrane and causing overactivation of intracellular malignant signaling. These intracellular effects of PC saturation are considered to confer resistance to AACOCF3, and it is not clear how to resolve this problem.

In this study, we characterized a potential target, DPP4, for the treatment of GBM, which could reverse PTRF−cPLA2 lipid remodeling inhibition to increase AACOCF3 chemo-resistance and be less ubiquitinated *via* binding to PTRF. In addition, there is a feedback loop between DPP4 and EGFR in which EGFR can increase the transcription of DPP4; in turn, DPP4 can prevent EGFR ubiquitination by competing with c-Cbl for binding with EGFR. Importantly, we discovered a noncanonical function of linagliptin: it disrupts the interaction between DPP4 and EGFR to promote EGFR degradation through the UPS. *In vivo*, linagliptin

truncation of EGFR was assessed by Co-IP assays with an anti-Flag antibody. (H) EGFR Co-IP in GBM cells treated with linagliptin (20 μmol/L) for 48 h followed by c-Cbl detection by immunoblotting. (I) mRNA levels of *EGFR* and *EGFR*vIII in GBM cells after 48 h of treatment with linagliptin (20 μmol/L). (J) WB analysis and quantification of EGFR/EGFRvIII degradation in cells treated with CHX alone or in combination with CHX and 20 μmol/L linagliptin for 24 h. (K) WB analysis of EGFR/EGFRvIII in U87-MG and TBD0220 cells treated with CHX, MG132, CQ, or 20 μmol/L linagliptin for 24 h. (L) Co-IP assays were conducted with an anti-EGFR antibody in GBM cells treated with 20 μmol/L linagliptin for 8 h, followed by immunoblotting with ubiquitin. Data are represented as mean ± SD; $n = 3$ independent experiments. $^{***}P < 0.001$; ns, no significance.

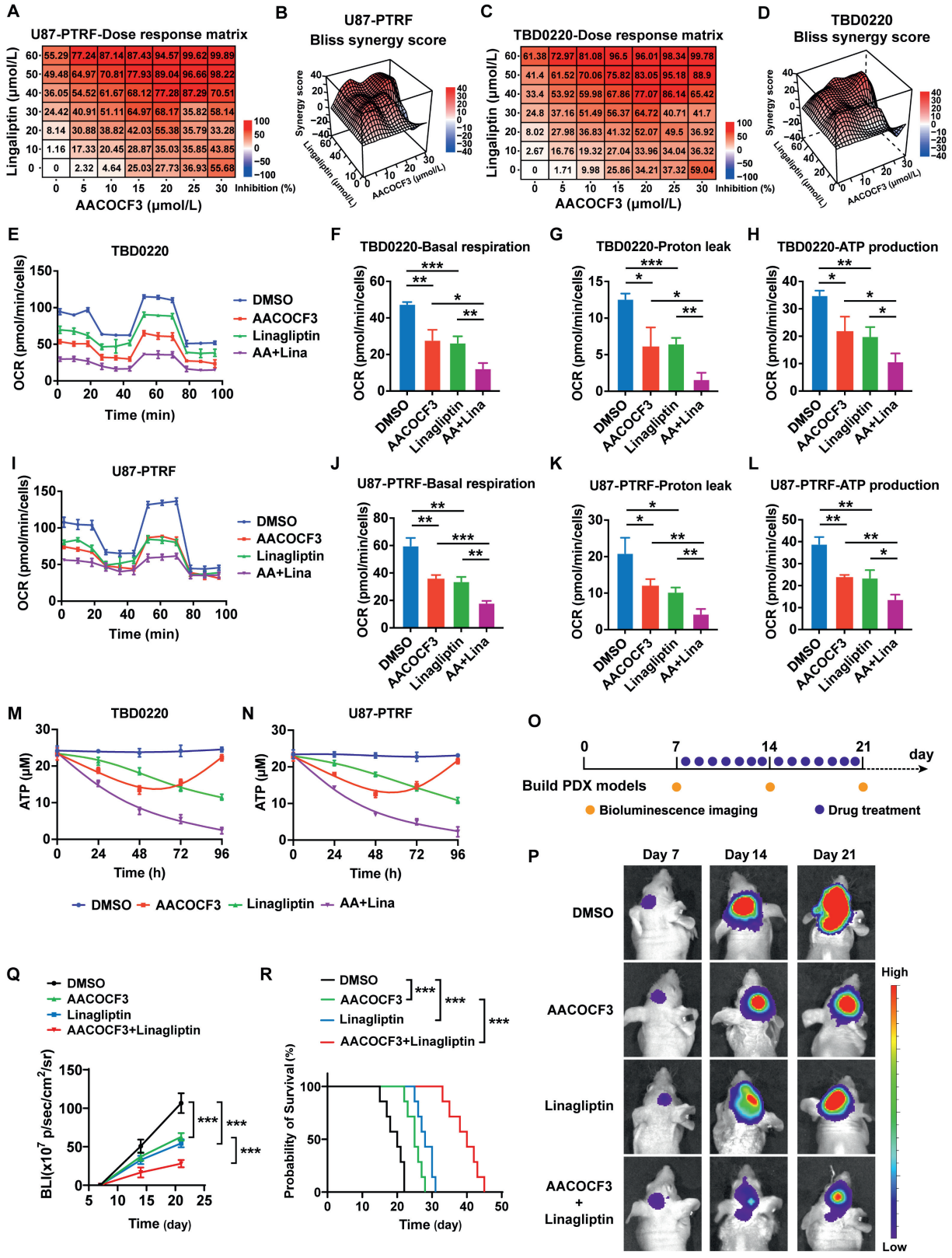

Figure 5 Linagliptin synergistically sensitizes GBM cells to AACOCF3 and inhibits energy metabolism and proliferation. (A) Dose−response matrix of linagliptin and AACOCF3 in U87-PTRF cells. (B) Bliss synergy score of linagliptin and AACOCF3 in U87-PTRF cells. (C) Dose−response matrix of linagliptin and AACOCF3 in TBD0220 cells. (D) Bliss synergy score of linagliptin and AACOCF3 in TBD0220 cells. (E) OCR curves of TBD0220 cells treated with DMSO, AACOCF3, linagliptin or a combination of AACOCF3 and linagliptin for 48 h for different durations were measured using a seahorse analyzer. (F−H) OCR measurements of (F) basal respiration, (G) proton leakage, and (H) ATP production in TBD0220 cells. (I) OCR curves of U87-PTRF cells treated with DMSO, AACOCF3, linagliptin or a combination of AACOCF3 and

also exhibited synergistic effects with AACOCF3 and TMZ. In summary, DPP4 functions as a potential target and stabilizer for EGFR, resulting in aberrant signal transduction, and linagliptin suppresses this process.

DPP4 is a membrane-bound protein present in various cell types, and its soluble form is found in bodily fluids. Evidence has long indicated varying degrees of CD26/DPP4 expression in different primary and metastatic tumors[29]. High DPP4 expression is indicative of a poor prognosis in lower-grade glioma patients[30]. Researchers have proposed that DPP4 inhibitor therapy can extend the survival of preclinical GBM models[31]. Linagliptin, recently approved as a DPP4 inhibitor, is widely recognized as a first-line treatment for type 2 diabetes patients[32,33]. Existing research predominantly focuses on the classical functions of linagliptin, while its nonclassical functions are somewhat unclear. Here, we explored that linagliptin could block the interaction between DPP4 and EGFR.

PTRF, also called Cavin1, is initially described as a transcription factor[34]. However, it is a special protein that functions in many biological processes, such as caveolae formation, extracellular vesicle genesis, transport, and secretion, phospholipid metabolism remodeling, and aerobic glycolysis[12,18,35,36]. In addition, PTRF can stabilize specific proteins and prevent their ubiquitination. In our previous study, we showed that PTRF could suppress the ubiquitination of cPLA2 and P4HA1 and stabilize them by interacting with them[12,18]. In this study, we observed that DPP4 was stabilized *via* interaction with PTRF and therefore could not be ubiquitinated. However, the exact amino acid residues and domains involved in the binding between DPP4 and PTRF need to be further investigated. Overall, our study provides novel details on PTRF function.

EGFR stability regulation is critical for sustaining abnormal EGFR signaling; however, the mechanisms underlying the proteasome-dependent degradation of EGFR are unclear. It has been reported that both lysosomal and proteasomal degradation are involved in regulating EGFR stability. Under EGF stimulation, EGFR degradation is suppressed by proteasome inhibitors and lysosome inhibitors. During lysosome-mediated degradation, tyrosine phosphorylation of EGFR and c-Cbl, ubiquitination of EGFR and proteasomal activity are vital for the transport of EGF and EGFR to lysosomes. In the absence of EGF stimulation, EGFR is degraded through the UPS, which is consistent with our results[19,20,37]. However, EGFR is a transmembrane protein, and the process by which ubiquitinated EGFR is released from the cytomembrane and transported to proteasomes is still unclear. In this study, we revealed that the AA 506−766 truncation of DPP4 bound to the Ex25−28 truncation of EGFR to prevent c-Cbl from interacting with EGFR, which decreased the ubiquitination level of EGFR. However, the exact conformation and whether key residues, such as Tyr1045 of EGFR and Tyr547, Tyr629, Tyr631, and Tyr662 of DPP4, are involved in the interaction between EGFR and DPP4 need to be further analyzed. These results provide supporting evidence for the protective effect of DPP4 and the blocking effect of linagliptin.

In addition, the combination of linagliptin and AACOCF3 can also enhance the therapeutic effect of TMZ and significantly prolong the survival of tumor-bearing mice treated with TMZ. The prognostic value of our PDP scoring system based on PTRF, DPP4, and PLA2G4A was well verified in TCGA and CGGA databases. This score can be used to stratify glioma patients according to prognosis. Based on this scoring system, patient treatment regimens can be adjusted accordingly, which might further optimize the application of TMZ combination regimens including AACOCF3 and linagliptin, and improve patient outcomes.

5. Conclusions

In conclusion, our study identifies DPP4 as a potential target and provides a novel therapy for the treatment of GBM. This study expanded our understanding of DPP4 and linagliptin functions and provides promising therapeutic approaches to treat not only GBM but also other cancers.

Acknowledgments

This study was supported by the National Key R&D Program of China, MOST (2023YFC2510000), the Key-Area Research and Development Program of Guangdong Province (2023B1111020008), and the National Natural Science Foundation of China (82373147 and 82473379).

Author contributions

Dongyuan Su: Writing − review & editing, Writing − original draft, Visualization, Methodology, Investigation, Formal analysis, Data curation, Conceptualization. Biao Hong: Writing − original draft, Visualization, Methodology, Investigation, Data curation. Shixue Yang: Methodology, Formal analysis, Data curation. Jixing Zhao: Validation, Methodology. Xiaoteng Cui: Methodology, Investigation. Qi Zhan: Methodology, Investigation. Kaikai Yi: Methodology, Investigation. Yanping Huang: Methodology, Investigation. Jiasheng Ju: Methodology, Investigation. Eryan Yang: Methodology, Investigation. Qixue Wang: Methodology, Investigation. Junhu Zhou: Methodology, Investigation. Yunfei Wang: Methodology, Investigation. Xing Liu: Writing − original draft, Visualization, Formal analysis, Data curation, Conceptualization. Chunsheng Kang: Supervision, Project administration, Funding acquisition, Conceptualization.

Conflicts of interest

The authors declare no competing interests.

linagliptin for 48 h for different durations were measured using a seahorse analyzer. (J−L) OCR measurements of (J) basal respiration, (K) proton leakage, and (L) ATP production in U87-PTRF cells. (M, N) ATP change curves of GBM cells treated with DMSO, linagliptin, AACOCF3, or linagliptin + AACOCF3 for 0−96 h. In (E, I, M, N), GBM cells were treated with 25 μmol/L AACOCF3, 20 μmol/L linagliptin, or 25 μmol/L AACOCF3 + 20 μmol/L linagliptin. (O) Tumor-bearing nude mice were treated with DMSO, AACOCF3 (25 mg/kg), linagliptin (15 mg/kg) or AACOCF3 (25 mg/kg) + linagliptin (15 mg/kg) by gavage. $n = 7$ for each group. (P) Bioluminescence images of representative mice from all groups. (Q) Quantification of bioluminescence intensity in all groups. *P*, two-way ANOVA. (R) Kaplan−Meier survival curves of nude mice. *P*, log-rank test. Data are represented as the mean ± SD; $n = 3$ independent experiments. $^{*}P < 0.05$, $^{**}P < 0.01$, and $^{***}P < 0.001$.

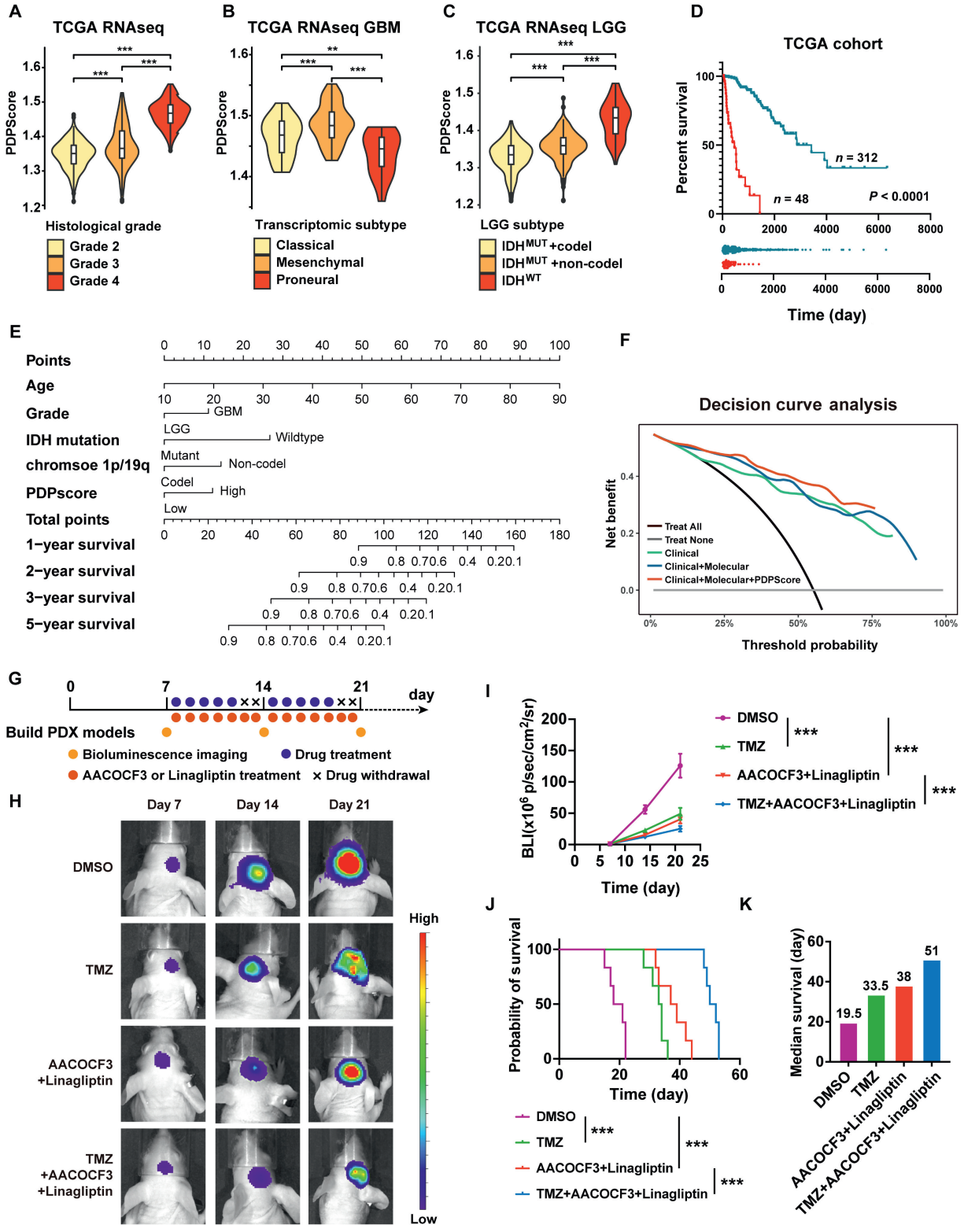

Figure 6 The combination of linagliptin and AACOCF3 can enhance the antitumor effect of TMZ *in vivo*. (A) PDP scores among patients with different histological grades in the TCGA database. (B) PDP scores among different transcriptomic subtypes in the TCGA database. (C) PDP scores among different LGG subtypes in the TCGA database. (D) Survival curves of patients with high and low PDP scores in the TCGA cohort. (E) A nomogram integrating prognostic characteristics in the TCGA cohort (c-index = 0.874). (F) Decision curve analysis revealed that the combination of clinical, molecular, and PDP-based scores provided the best prognosis. (G) Tumor-bearing nude mice were treated with DMSO, TMZ (5 mg/kg), AACOCF3 (25 mg/kg) + linagliptin (15 mg/kg), or TMZ (5 mg/kg) + AACOCF3 (25 mg/kg) + linagliptin (15 mg/kg) by gavage. $n = 6$ for each group. (H) Bioluminescence images of representative mice from all groups. (I) Quantification of bioluminescence intensity in all groups. *P*, two-way ANOVA. (J) Kaplan−Meier survival curve of nude mice. *P*, log-rank test. (K) Median survival of all groups. Data are represented as the mean ± SD; $n = 3$ independent experiments. $^{**}P < 0.01$ and $^{***}P < 0.001$.

Appendix A. Supporting information

Supporting information to this article can be found online at https://doi.org/10.1016/j.apsb.2025.05.012.

References

1. Lin H, Liu C, Hu A, Zhang D, Yang H, Mao Y. Understanding the immunosuppressive microenvironment of glioma: mechanistic insights and clinical perspectives. *J Hematol Oncol* 2024;**17**:31.
2. Ostrom QT, Price M, Neff C, Cioffi G, Waite KA, Kruchko C, et al. CBTRUS statistical report: primary brain and other central nervous system tumors diagnosed in the United States in 2015−2019. *Neuro Oncol* 2022;**24**:v1−95.
3. Li W, Cai H, Ren L, Yang Y, Yang H, Liu J, et al. Sphingosine kinase 1 promotes growth of glioblastoma by increasing inflammation mediated by the NF-κB/IL-6/STAT3 and JNK/PTX3 pathways. *Acta Pharm Sin B* 2022;**12**:4390−406.
4. Wen PY, Weller M, Lee EQ, Alexander BM, Barnholtz-Sloan JS, Barthel FP, et al. Glioblastoma in adults: a society for neuro-oncology (SNO) and European society of neuro-oncology (EANO) consensus review on current management and future directions. *Neuro Oncol* 2020;**22**:1073−113.
5. Weller M, van den Bent M, Preusser M, Le Rhun E, Tonn JC, Minniti G, et al. EANO guidelines on the diagnosis and treatment of diffuse gliomas of adulthood. *Nat Rev Clin Oncol* 2021;**18**:170−86.
6. Liu H, Qiu W, Sun T, Wang L, Du C, Hu Y, et al. Therapeutic strategies of glioblastoma (GBM): the current advances in the molecular targets and bioactive small molecule compounds. *Acta Pharm Sin B* 2022;**12**:1781−804.
7. Wang B, Rong X, Palladino END, Wang J, Fogelman AM, Martín MG, et al. Phospholipid remodeling and cholesterol availability regulate intestinal stemness and tumorigenesis. *Cell Stem Cell* 2018;**22**:206−20.
8. Morita Y, Sakaguchi T, Ikegami K, Goto-Inoue N, Hayasaka T, Hang VT, et al. Lysophosphatidylcholine acyltransferase 1 altered phospholipid composition and regulated hepatoma progression. *J Hepatol* 2013;**59**:292−9.
9. Slatter DA, Aldrovandi M, O'Connor A, Allen SM, Brasher CJ, Murphy RC, et al. Mapping the human platelet lipidome reveals cytosolic phospholipase A2 as a regulator of mitochondrial bioenergetics during activation. *Cell Metab* 2016;**23**:930−44.
10. Carracedo A, Cantley LC, Pandolfi PP. Cancer metabolism: fatty acid oxidation in the limelight. *Nat Rev Cancer* 2013;**13**:227−32.
11. Huang K, Fang C, Yi K, Liu X, Qi H, Tan Y, et al. The role of PTRF/Cavin1 as a biomarker in both glioma and serum exosomes. *Theranostics* 2018;**8**:1540−57.
12. Yi K, Zhan Q, Wang Q, Tan Y, Fang C, Wang Y, et al. PTRF/cavin-1 remodels phospholipid metabolism to promote tumor proliferation and suppress immune responses in glioblastoma by stabilizing cPLA2. *Neuro Oncol* 2021;**23**:387−99.
13. Harayama T, Riezman H. Understanding the diversity of membrane lipid composition. *Nat Rev Mol Cell Biol* 2018;**19**:281−96.
14. Bi J, Ichu TA, Zanca C, Yang H, Zhang W, Gu Y, et al. Oncogene amplification in growth factor signaling pathways renders cancers dependent on membrane lipid remodeling. *Cell Metab* 2019;**30**:525−38.
15. Joung J, Konermann S, Gootenberg JS, Abudayyeh OO, Platt RJ, Brigham MD, et al. Genome-scale CRISPR-Cas9 knockout and transcriptional activation screening. *Nat Protoc* 2017;**12**:828−63.
16. Li W, Köster J, Xu H, Chen C-H, Xiao T, Liu JS, et al. Quality control, modeling, and visualization of CRISPR screens with MAGeCK-VISPR. *Genome Biol* 2015;**16**:281.
17. Zheng S, Wang W, Aldahdooh J, Malyutina A, Shadbahr T, Tanoli Z, et al. SynergyFinder plus: toward better interpretation and annotation of drug combination screening datasets. *Genom Proteom Bioinform* 2022;**20**:587−96.
18. Yang S, Zhan Q, Su D, Cui X, Zhao J, Wang Q, et al. HIF1alpha/ATF3 partake in PGK1 K191/K192 succinylation by modulating P4HA1/succinate signaling in glioblastoma. *Neuro Oncol* 2024;**26**:1405−20.
19. Niu M, Xu J, Liu Y, Li Y, He T, Ding L, et al. FBXL2 counteracts Grp94 to destabilize EGFR and inhibit EGFR-driven NSCLC growth. *Nat Commun* 2021;**12**:5919.
20. Levkowitz G, Waterman H, Ettenberg SA, Katz M, Tsygankov AY, Alroy I, et al. Ubiquitin ligase activity and tyrosine phosphorylation underlie suppression of growth factor signaling by c-Cbl/Sli-1. *Mol Cell* 1999;**4**:1029−40.
21. Eckhardt M, Langkopf E, Mark M, Tadayyon M, Thomas L, Nar H, et al. 8-(3-(*R*)-Aminopiperidin-1-yl)-7-but-2-ynyl-3-methyl-1-(4-methyl-quinazolin-2-ylmethyl)-3,7-dihydropurine-2,6-dione (BI 1356), a highly potent, selective, long-acting, and orally bioavailable DPP-4 inhibitor for the treatment of type 2 diabetes. *J Med Chem* 2007;**50**:6450−3.
22. Mellinghoff IK, Cloughesy TF. Balancing risk and efficiency in drug development for rare and challenging tumors: a new paradigm for glioma. *J Clin Oncol* 2022;**40**:3510−9.
23. Schaff LR, Mellinghoff IK. Glioblastoma and other primary brain malignancies in adults. *JAMA* 2023;**329**:574−87.
24. Pavlova NN, Thompson CB. The emerging hallmarks of cancer metabolism. *Cell Metab* 2016;**23**:27−47.
25. Xia L, Oyang L, Lin J, Tan S, Han Y, Wu N, et al. The cancer metabolic reprogramming and immune response. *Mol Cancer* 2021;**20**:28.
26. Liao M, Yao D, Wu L, Luo C, Wang Z, Zhang J, et al. Targeting the Warburg effect: a revisited perspective from molecular mechanisms to traditional and innovative therapeutic strategies in cancer. *Acta Pharm Sin B* 2024;**14**:953−1008.
27. Jin HR, Wang J, Wang ZJ, Xi MJ, Xia BH, Deng K, et al. Lipid metabolic reprogramming in tumor microenvironment: from mechanisms to therapeutics. *J Hematol Oncol* 2023;**16**:103.
28. Hilvo M, Denkert C, Lehtinen L, Müller B, Brockmöller S, Seppänen-Laakso T, et al. Novel theranostic opportunities offered by characterization of altered membrane lipid metabolism in breast cancer progression. *Cancer Res* 2011;**71**:3236−45.
29. Enz N, Vliegen G, De Meester I, Jungraithmayr W. CD26/DPP4—a potential biomarker and target for cancer therapy. *Pharmacol Ther* 2019;**198**:135−59.
30. Han Y, Sun Y, Zhang Y, Xia Q. High DPP4 expression predicts poor prognosis in patients with low-grade glioma. *Mol Biol Rep* 2020;**47**:2189−96.
31. Bayik D, Bartels CF, Lovrenert K, Watson DC, Zhang D, Kay K, et al. Distinct cell adhesion signature defines glioblastoma myeloid-derived suppressor cell subsets. *Cancer Res* 2022;**82**:4274−87.
32. Kornelius E, Lin CL, Chang HH, Li HH, Huang WN, Yang YS, et al. DPP-4 inhibitor linagliptin attenuates Aβ-induced cytotoxicity through activation of AMPK in neuronal cells. *CNS Neurosci Ther* 2015;**21**:549−57.
33. Xie Y, Zhou Q, He Q, Wang X, Wang J. Opportunities and challenges of incretin-based hypoglycemic agents treating type 2 diabetes mellitus from the perspective of physiological disposition. *Acta Pharm Sin B* 2023;**13**:2383−402.
34. Bastiani M, Parton RG. Caveolae at a glance. *J Cell Sci* 2010;**123**:3831−6.
35. Hill MM, Bastiani M, Luetterforst R, Kirkham M, Kirkham A, Nixon SJ, et al. PTRF-Cavin, a conserved cytoplasmic protein required for caveola formation and function. *Cell* 2008;**132**:113−24.
36. Wang L, Yang C, Wang Q, Liu Q, Wang Y, Zhou J, et al. Homotrimer cavin1 interacts with caveolin1 to facilitate tumor growth and activate microglia through extracellular vesicles in glioma. *Theranostics* 2020;**10**:6674−94.
37. Longva KE, Blystad FD, Stang E, Larsen AM, Johannessen LE, Madshus IH. Ubiquitination and proteasomal activity is required for transport of the EGF receptor to inner membranes of multivesicular bodies. *J Cell Biol* 2002;**156**:843−54.